PRACTICAL ELECTRON MICROSCOPY IN MATERIALS SCIENCE

Monograph Three

3 Interpretation of Transmission Electron Micrographs

J W Edington

Philips Technical Library

Monographs in Practical Electron Microscopy in Materials Science

3

INTERPRETATION OF TRANSMISSION ELECTRON MICROGRAPHS

J. W. EDINGTON

Department of Metallurgy and Materials Science, University of Cambridge, Cambridge, England

SBN 333 18575 7

First published 1975 by

THE MACMILLAN PRESS LTD

London and Basingstoke
Associated companies in New York, Dublin,
Melbourne, Johannesburg and Madras

PHILIPS

Filmset at The Universities Press, Belfast, Northern Ireland
and printed by Thomson Litho Ltd., East Kilbride, Scotland

PREFACE

This is the third of a series of monographs on electron microscopy aimed at users of the equipment. They are written as both texts and sources of reference emphasising the applications of electron microscopy to the characterisation of materials.

In some places the author has referred the reader to material appearing in other monographs of this series. The following titles have already been published:

1. The Operation and Calibration of the Electron Microscope
2. Electron Diffraction in the Electron Microscope

and in preparation is:

4. Typical Electron Microscope Investigations

Abbreviations and Symbols Frequently Used in this Monograph

BF	Bright field (image)
DF	Dark field (image)
CDF	Centred dark field (image)
WB	Weak beam (image)
DP	Diffraction pattern
SADP	Selected area diffraction pattern
SRO	Short-range order
APB	Antiphase domain boundary
$\boldsymbol{g}$	A vector normal to the reflecting plane
s	The deviation from the Bragg reflection position
ξ_g	The extinction distance
w	$s\xi_g$
$\boldsymbol{b}$	The Burgers vector of an undissociated dislocation
$\boldsymbol{b}_p$	The Burgers vector of a partial dislocation
$\boldsymbol{\mu}$	The line vector of a dislocation
FN	The upward drawn foil normal (normal to the specimen surface)
$\boldsymbol{B}$	The upward drawn incident beam direction in the specimen, that is opposite to the direction of the electron beam
ANO	Anomalous absorption coefficient

CONTENTS

3. INTERPRETATION OF TRANSMISSION ELECTRON MICROGRAPHS

3. INTERPRETATION OF TRANSMISSION ELECTRON MICROGRAPHS

3.1 Image Contrast

There are two important mechanisms which produce image contrast in the electron microscope.

(1) *Diffraction contrast.* Diffracted electrons leaving the lower surface of a crystalline specimen are intercepted by the objective aperture and prevented from contributing to the image. Alternatively only one diffracted beam forms the image. See bright field (BF) and dark field (DF) images, section 1.

(2) *Phase contrast.* Some of the electrons leaving the specimen are recombined to form the image so that phase differences present at the exit surface of the specimen are converted into intensity differences in the image.

Diffraction contrast is the dominant mechanism delineating object detail $\gtrsim 15$ Å in crystalline specimens and is the most important and widely used contrast mechanism for study of crystal defects. Using this approach considerable quantitative information about the defect structure of the specimen may be obtained without operating the microscope at maximum resolution. Consequently, the technique is experimentally easy. Phase contrast is the dominant mechanism for object detail $\lesssim 10$ Å and is important in lattice resolution studies and investigations of the early stages of short-range order and amorphous materials. Here each contrast mechanism is discussed in simple terms, followed by a detailed treatment of the results of its application to the analysis of crystal defects. At present most quantitative work relies primarily on diffraction contrast; consequently the emphasis lies heavily in this area.

I. DIFFRACTION CONTRAST

3.2 Summary of Theory

Quantitative analysis of crystal defects using the diffraction contrast approach usually involves detailed comparison of BF and DF images. BF images exclude diffracted, and DF images transmitted, electrons. Consequently, they are simply high-magnification maps of the intensity distribution across the transmitted or diffracted beams produced by the interaction of the specimen illuminated with the incident electron beam. Thus image contrast arises from point-to-point differences in the efficiency of the diffraction process in the region of the specimen under study. As a result, the details of the image must be interpreted in terms of a suitable diffraction theory, which has been described in detail in a number of books, for example Amelinckx (1964), Heidenreich (1964), Hirsch *et al.* (1967), Amelinckx *et al.* (1970), Murr (1971) and Valdre and Zichichi (1971), and review articles, for example Whelan (1970) and Howie (1971), to which the reader is referred for detailed theoretical background. Here we emphasise the important conclusions of the theory for images of specific types of crystal defect and describes those image features which may be used to characterise the defects under study. Only the basic concepts of diffraction theory are included so that those factors important to the experimentalist may be defined.

Electron microscope images are normally discussed in terms of the dynamical theory of electron diffraction which incorporates as a special case the kinematical theory used in section 2 to describe electron diffraction patterns. The dynamical theory more accurately describes the diffraction process occurring in the electron microscope specimen and has been developed for the interpretation of image contrast in the electron microscope in a series of papers by Hirsch, Howie, Whelan, Amelinckx, Gevers, van Landuyt and their coworkers. The details of the theory have been summarised in the books referred to above. The simplest form of the theory only considers the case of two beams—one transmitted through, and one diffracted by, the specimen. The following factors not included in the kinematical theory of section 2 are incorporated in the dynamical theory.

(1) The intensity in the diffracted beam may be high compared with the transmitted beam.

(2) Electrons may be redIffracted back from the diffracted into the transmitted beam.

(3) Absorption of the electrons by the specimen, that is there is a limitation on penetration.

A more detailed formulation of the theory which includes several diffracted beams, the 'multi-beam' case, is summarised in the review articles by Howie (1970) and Goringe (1971). This is important for accelerating voltages $\gtrsim 300$ kV when two-beam conditions may be difficult to obtain for metallic specimens.

3.2.1 *The Perfect Crystal*

The simple two-beam dynamical theory describes the amplitudes ϕ_0 (transmitted) and ϕ_g (diffracted) in an element dz, depth z, in a small column of material in a thin foil thickness t, see figure 3.1. This theory assumes the following.

(1) The column is narrower than the image but wide enough to contain both the diffracted and transmitted amplitudes. This is possible because the scattering angle for 100 kV electrons is small ($2\theta \lesssim 1°$).

(2) There is no contribution to the waves in the column from the rest of the specimen and conversely no loss from the column to the specimen.

(3) If the crystal is distorted, that is when a crystal defect is present (see section 3.2.4), the distortion occurs down but not across the column.

(4) Only plane waves exist in the column.

(5) Only one diffracted beam exists, that is *two-beam conditions*, see figure 2.35.

Points (1)–(3) are known as the column approximation and have been justified in the case of single dislocations by Jouffrey and Taupin (1967) and Howie and Basinski (1968) and for narrow dipoles near the foil surface by Colliex *et al.* (1969). Point (5) is more important because it specifies that images to be analysed quantitatively must *always* be produced under two-beam conditions.

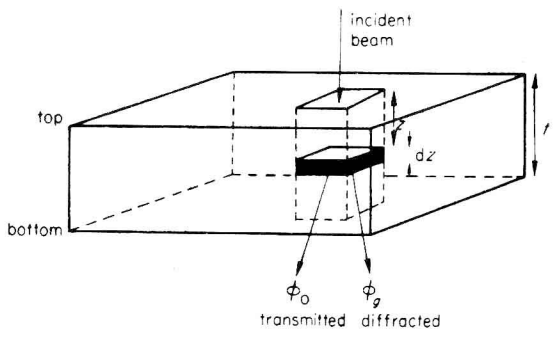

Figure 3.1 The column approximation for a perfect crystal

The theory allows for contribution back to the transmitted beam from the diffracted beam. Thus, as the transmitted wave propagates into the crystal, its amplitude ϕ_0 will be depleted by diffraction while the amplitude of ϕ_g is increased correspondingly, that is there is coupling between ϕ_0 and ϕ_g. The coupling is described by a pair of differential equations known as the Darwin–Howie–Whelan equations:

$$\frac{d\phi_0}{dz} = \frac{i\pi}{\xi_0}\phi_0 + \frac{i\pi}{\xi_g}\phi_g \exp(2\pi i s z)$$
$$\frac{d\phi_g}{dz} = \frac{i\pi}{\xi_0}\phi_0 \exp(-2\pi i s z) + \frac{i\pi}{\xi_g}\phi_g \qquad (3.1)$$

where s is the deviation from the exact Bragg angle, see figure 2.16, and ξ_0 and ξ_g are constants. The term ξ_g describes a critical distance in the perfect crystal at which the transmitted intensity falls to zero before increasing again and is known as the extinction distance, see section 3.2.3.1 for more details. The term $\exp(2\pi i s z)$ represents a phase factor arising from the scattering process. The first of these equations states that the change in ϕ_0 in depth dz is partly due to forward scattering by the atoms in the element dz and partly due to scattering from the diffracted beam. Furthermore, there is a phase change of $\pi/2$, represented by the factor i, which arises from the scattering process.

3.2.2 *Absorption*

Two types of absorption need to be considered: (a) uniform absorption which leads to an overall decrease in intensity with increasing depth and (b) anomalous absorption which involves selective absorption of some electrons within the crystal and is responsible for some of the important depth asymmetry of many of the images of crystal defects discussed in subsequent sections.

Anomalous and uniform absorption are allowed for mathematically by introducing an imaginary component into the parameters $1/\xi_g \rightarrow 1/\xi_g + i/\xi'_g$, and $1/\xi_0 \rightarrow 1/\xi_0 + i/\xi'_0$, respectively. The term ξ_0/ξ'_0 is the uniform absorption parameter which influences the overall background intensity of the image. The term ξ_g/ξ'_g is the anomalous absorption parameter (ANO) which is responsible for many of the detailed features of diffraction contrast images. The value of ANO has been generally taken as 0.1 but Humphreys and Hirsch (1968) have pointed out that it is a function of both atomic weight and operative reflection and that this should be taken into account in some cases where accurate computation of images is necessary, for example sections 3.4–3.6.

3.2.3 *Characteristic Images of Perfect Crystals*

There are four types of image that are not related to the defect content of thin foils and are therefore found in almost all electron microscope specimens. These are (a) thickness fringes, (b) bend extinction contours, (c) bend contours and (d) bend centres, the details of which are most easily seen in annealed single-phase materials with a low defect density.

3.2.3.1 *Thickness fringes*

The depth variation of the transmitted intensity in a perfect crystal under dynamical diffracting conditions may be obtained from equations (3.1) and it can be shown that the diffracted intensity is

$$|\phi_g|^2 = \frac{\pi^2}{\xi_g^2} \frac{\sin^2(\pi t s_{\text{eff}})}{(\pi s_{\text{eff}})^2} \tag{3.2}$$

and the transmitted intensity is

$$|\phi_0|^2 = (1 - |\phi_g|^2)$$

where $s_{\text{eff}} = (s^2 + \xi_g^{-2})^{1/2}$. The intensity oscillates with depth as shown in figure 3.2(a) with a periodicity of ξ_g which is known as the extinction distance. It is clear from figure 3.2(a) that the transmitted intensity is zero for specimen thickness $(n + \frac{1}{2})\xi_g$, where n is an integer. Consequently the edge of a typical wedge-shaped electropolished foil exhibits dark fringes connecting regions of the same thickness $\frac{1}{2}\xi_g$, $1\frac{1}{2}\xi_g$, $2\frac{1}{2}\xi_g$, etc., see figure 3.2(b), (c). However, when absorption is allowed for, the fringes are damped with increasing thickness and disappear before the transmitted intensity is zero, see figure 3.2(d). This often occurs above ~5 fringes. Clear high-contrast images of crystal defects are generally obtained at thicknesses where the thickness fringes just damp out, see figure 3.2(d). The thickness fringes show opposite contrast in dark field, compare figures 3.2(d), (e). Under kinematical conditions these thickness fringes almost disappear, as described later in this section.

The extinction distance ξ_g depends on both the operative reflection and the deviation from the exact Bragg position. The value of ξ_g at $s = 0$ may be calculated from the relationship

$$\xi_g = \frac{\pi \Omega \cos\theta}{\lambda f(\theta)} \tag{3.3}$$

where $f(\theta)$ is the atomic scattering amplitude obtained from the tables in appendix 8, θ is the Bragg angle, Ω is the volume of the unit cell and λ is the electron wavelength. Appendix 10 gives typical values of ξ_g for various metals to an accuracy $\pm 10\%$ because of inaccuracies in $f(\theta)$. Note that ξ_g increases with increasing order of reflection because $f(\theta)$ decreases as θ increases. If $s \neq 0$ then we have an effective extinction distance $\xi_{g\,\text{eff}} = \xi_g/(1 + s^2\xi_g^2)^{1/2}$, that is ξ_g decreases with deviation from the Bragg position. Thus the spacing of the extinction fringes in an electron microscope image change if the operative reflection is changed by tilting the specimen or if s varies from point to point in the specimen because of bending of the foil.

Under kinematical conditions $s \gg 1/\xi_g$ and $s_{\text{eff}} \approx s$. Thus equation (3.2) reduces to

$$|\phi_g|^2 = \frac{\pi^2}{\xi_g^2} \frac{\sin^2(\pi t s)}{(\pi s)^2} \tag{3.4}$$

which has the form shown in figure 3.2(f). In this case there are weak thickness fringes in the bright field image, figure 3.2(g), but stronger thickness fringes occur in the dark field image, see figure 3.2(h). However, in this case the extinction distance is $\ll \xi_g$ calculated for $s = 0$, and the fringes are closer together.

3.2.3.2 *Bend extinction contours*

This phenomenon occurs if the foil is elastically bent about a large radius like the top of a cylindrical pipe, as shown in figure 3.3(a). The $\{hkl\}$ family of reflecting planes on the right will be tilted away from the exact Bragg position by an amount depending on the distance from the point where $s = 0$ at position O. Figures 3.3(b), (c) show schematically the intensity distribution in both the transmitted beam (bright field image) and diffracted beam (dark field image) as a function of distance from O.

In this case distance is described more conveniently in terms of the deviation from the Bragg position by the parameter $w = s\xi_g$ and the graph is termed a 'rocking curve'.

The following conclusions may be drawn, figure 3.3(b).

(1) The bright field intensity depends on the sign of s (rocking curve asymmetrical about O) whereas the dark field image does not (rocking curve symmetrical about O).

(2) When s is small and positive there is a region of high transmitted intensity in bright field (termed anomalous transmission).

(3) When s is negative, overall transmission is very low in bright field.

(4) In dark field best transmission occurs at $s \approx 0$.

(5) On the left of figure 3.3(a), the same planes reflect but from their other side, that is they are now $\{\bar{h}\bar{k}\bar{l}\}$. Conclusions (1)–(4) above apply, see figure 3.3(c).

A typical example of a bend extinction contour is shown in figure 3.3(d). Note that diffraction patterns taken from points X and Y, figure 3.3(e), show (hkl) and $(\bar{h}\bar{k}\bar{l})$ reflections as indicated in

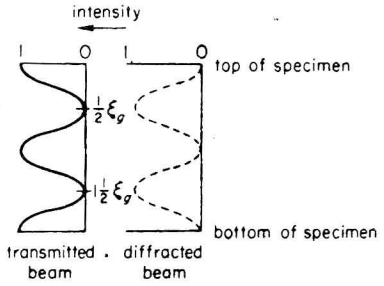

(a)

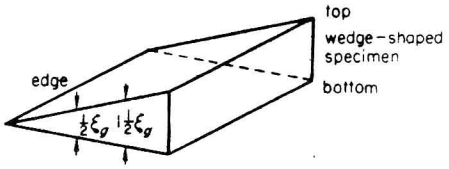

(b)

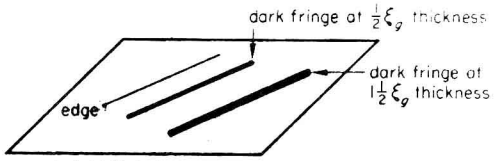

(c)

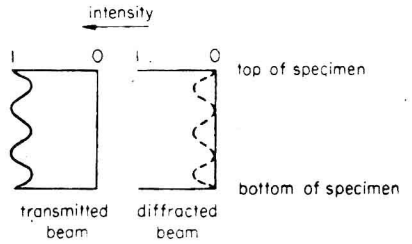

(f)

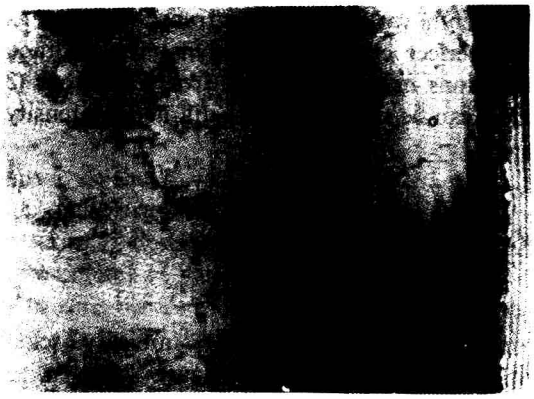

(g)

(d)

(h)

(e)

1 μm

increasing thickness edge

Figure 3.2 (a) The intensity distribution of the transmitted (BF) and diffracted (DF) beams with depth, according to equation (3.2) (dynamical). (b) A schematic diagram of a wedge-shaped defect-free specimen. (c) The positions of the thickness fringes in the image. (d) and (e) BF and CDF dynamical images of the same area of a wedge-shaped aluminium foil showing dislocations and thickness fringes. (f) The intensity distribution versus depth for the transmitted (BF) and diffracted (DF) beams according to equation (3.4) (kinematical). (g) and (h) BF and CDF kinematical images of the same area as (e), (f) showing dislocations but with only faint thickness fringes in BF

figure 3.3(b), (c). The edge of the specimen is visible and thickness increases on moving into the specimen. The line AOA′ in figure 3.3(d) corresponds approximately to the intensity graph in figure 3.3(b), and fringes are clearly visible on travelling from O → A′. However, for the thicker regions in figure 3.3(d) these fringes are weaker because of increased absorption. The region of s small and positive corresponds to the normal region in which bright field photographs are taken because of the good transmission. In addition when s is negative the background intensity in bright field is low, see centre of bend extinction contour in figure 3.3(d). When the specimen is tilted, the bend extinction contour will move slowly across the field of view at low magnifications ($\lesssim$15 000).

3.2.3.3 *Bend contours*

In very thin regions of the foil where the kinematical theory applies and absorption can be ignored, bending often occurs over relatively short distances producing diffuse dark lines in the bright field image, see lines AA′ in figure 3.4(a). These fringes are usually ~500 Å wide and may be recognised because they move rapidly across the field of view when the specimen is tilted through a small angle. The sign of s changes from side to side of a bend contour.

3.2.3.4 *Bend centres*

For beam directions exactly parallel to simple crystallographic directions, characteristic bend extinction contour images occur in thin regions of bent foils. Examples are shown in figure 3.4(b)–(g) for different beam directions in the f.c.c. crystal structure. Each long arm of the image corresponds to an individual bend extinction contour and the point at the centre of all the arms is the exact orientation, $\boldsymbol{B}$ parallel to the specific crystal directions with all spots in the diffraction pattern equally bright. In order to produce such an image the specimen is elastically bent into an approximately spherical shape.

Such bend centres are used to compare the influence of operating reflections on the form of the image of crystal defects such as precipitates or for tilting specific $\boldsymbol{B}$ for comparison with a set of standard diffraction patterns.

3.2.4 *Crystal Containing a Defect with a Strain Field*

In general, thin electron microscope specimens contain a number of defects such as dislocations, stacking faults, precipitates, etc. Using the case

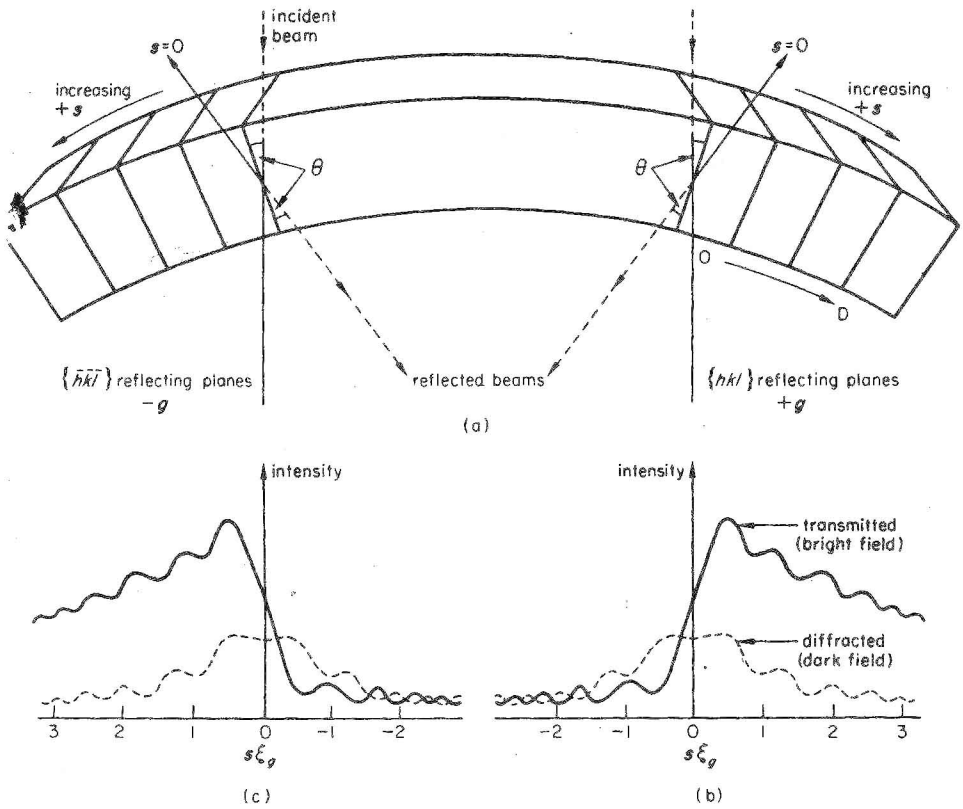

Figure 3.3 (a) A thin crystal bent into a large radius showing reflection from the opposite sides of the same set of (*hkl*) crystal planes. (b), (c) The intensity distribution versus position for BF and DF (rocking curves). (d) The BF image corresponding to (a). (e), (f) are SADPs showing opposite two-beam diffracting conditions at Y and X in (d)

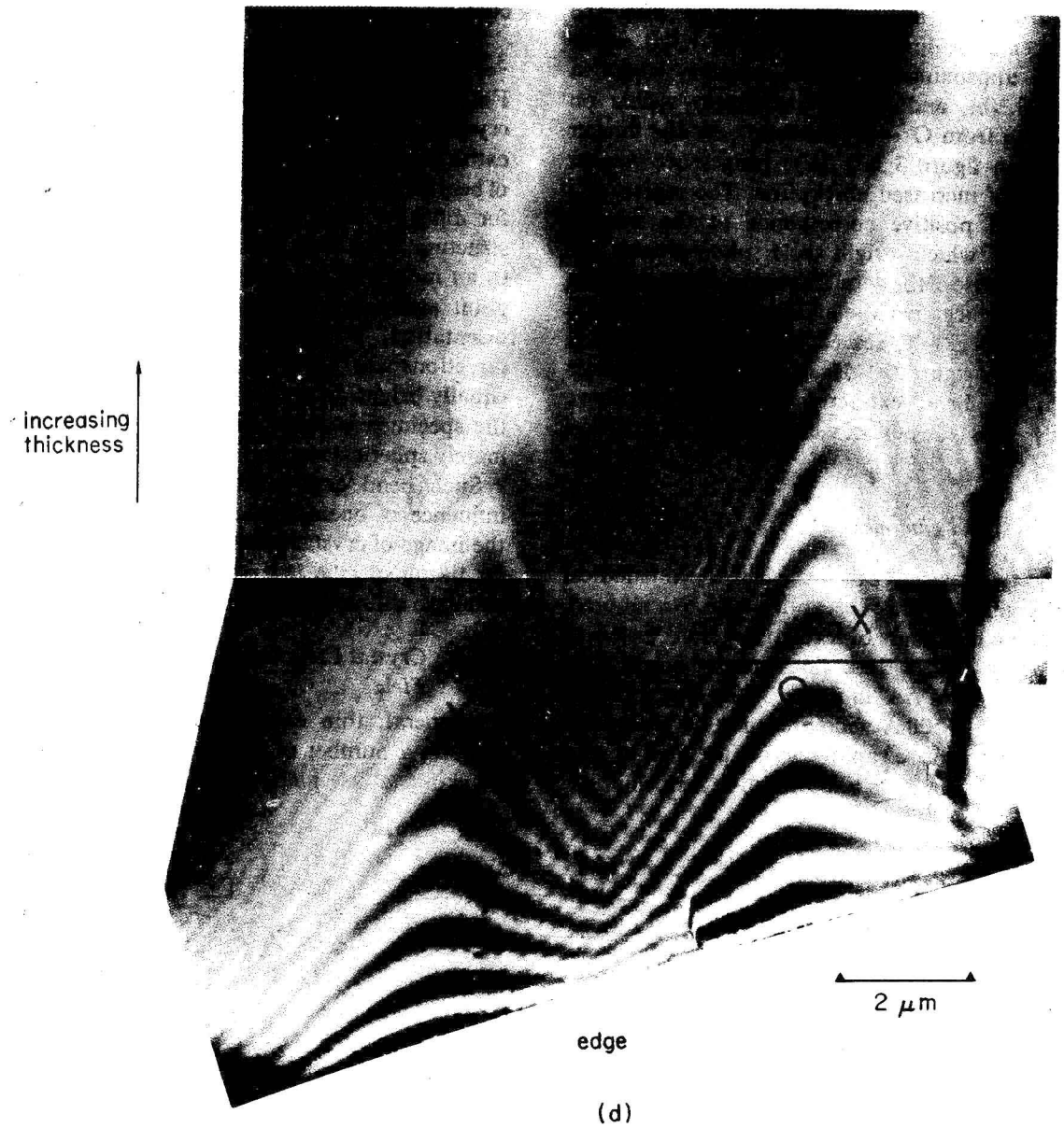

(d)

($\bar{1}\bar{1}\bar{1}$) beam

(e)

(111) beam

(f)

Figure 3.3 (*continued*)

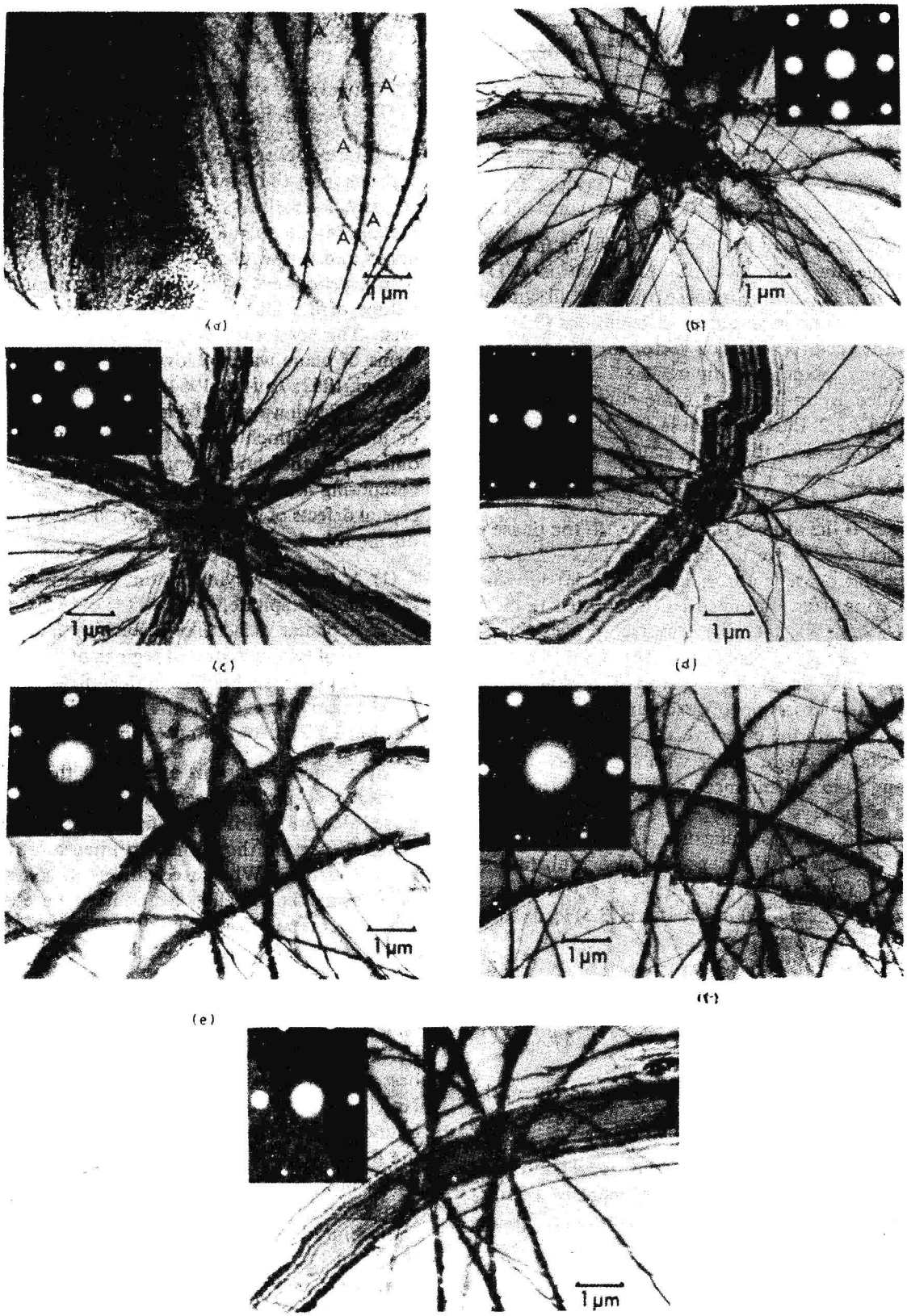

Figure 3.4 (a) Bend contours AA′ and bend centres in aluminium with associated SADP inset, (b) [100], (c) [110], (d) [112], (e) [111], (f) [114], (g) [013]

of a dislocation as an example, see figure 3.5(a), the equations corresponding to equations (3.1) are

$$\frac{d\phi_0}{dz} = \frac{i\pi}{\xi_0}\phi_0 + \frac{i\pi}{\xi_g}\phi_g \exp(2\pi isz + 2\pi i\boldsymbol{g}\cdot\boldsymbol{R}) \tag{3.5a}$$

$$\frac{d\phi_g}{dz} = \frac{i\pi}{\xi_g}\phi_0 \exp(-2\pi isz - 2\pi i\boldsymbol{g}\cdot\boldsymbol{R}) + \frac{i\pi}{\xi_g}\phi_g \tag{3.5b}$$

if the displacement in the column arising from, for example, the strain field of the dislocation at DD in figure 3.5(a) is $\boldsymbol{R}(z)$. In these equations all symbols have the same meaning as in equations (3.1) and $\boldsymbol{g}$ is the reciprocal lattice vector for the operative reflecting plane, see figure 2.8. Absorption is included by making the same substitution as in section 3.2.2. Effectively these equations mean that the distortion of the lattice causes a phase factor $\exp(-i\alpha)$, where $\alpha = 2\pi\boldsymbol{g}\cdot\boldsymbol{R}$, to be superimposed on the normal scattering process for the perfect crystal. If the atom is displaced by $\boldsymbol{R}$, the phase of the scattered wave is changed by $\exp(-2\pi\boldsymbol{g}\cdot\boldsymbol{R})$. Since this phase factor in equation (3.5a) describes scattering from diffracted to transmitted beam as $\exp(+2\pi\boldsymbol{g}\cdot\boldsymbol{R})$ for the reverse process it is $\exp(-2\pi\boldsymbol{g}\cdot\boldsymbol{R})$ in equation (3.5b). Thus, when we form a BF image of a distorted crystal in the electron microscope by excluding the diffracted electrons with the objective aperture, section 1.5.2, we obtain a bright image with some dark regions arising from the enhanced diffraction by the strain field of the crystal defect.

The physical significance of equations (3.5) may be made clear as follows. Substituting $\phi'_0 = \phi_0(z)\exp(-\pi iz/\xi_0)$ and $\phi'_g = \phi_g(z)\exp(2\pi isz - \pi iz/\xi_0 + 2\pi i\boldsymbol{g}\cdot\boldsymbol{R})$ in equations (3.5) leads to

$$\frac{d\phi'_0}{dz} = \frac{\pi i}{\xi_g}\phi'_g \tag{3.6a}$$

$$\frac{d\phi'_g}{dz} = \frac{\pi i}{\xi_g}\phi'_0 + \left(2\pi is + 2\pi i\boldsymbol{g}\cdot\frac{d\boldsymbol{R}}{dz}\right)\phi'_g \tag{3.6b}$$

Thus the strain field of the dislocation enters the equation as $\boldsymbol{g}\cdot(d\boldsymbol{R}/dz)$ and acts like a local rotation of the reflecting planes which changes the value of s. Consequently the local diffracted intensity can be considered to increase because the local Ewald sphere construction passes nearer the $s = 0$ position in reciprocal space, see figure 2.16.

Of course the above approach also enables strain-free situations to be described in which the phase factor α arises from the simple displacement of one part of the crystal relative to another, by a vector $\boldsymbol{R}$, such as occurs in the case of stacking faults, see section 3.6.

Note that the characteristic features of a perfect crystal (section 3.2.3) will also be present but the details may be destroyed if a high density of crystal defects is present.

3.3 Relevance of Diffraction Theory to Studies of Crystal Defects

The differential equations described in the previous sections form the basis for the calculation of image contrast for diffraction images of crystal defects. Details of the calculations may be found in the books and review papers listed in section 3.2.

In practice several physically equivalent formulations of the Darwin–Howie–Whelan equations exist. The scattering may be described either in terms of plane waves (Howie and Whelan, 1961; Takagi, 1962; Taupin, 1964), as for equations (3.1), (3.5), or Bloch waves (Howie, 1963; Wilkens, 1964) or modified Bloch waves (Wilkens, 1966). These different mathematical expressions are all used for computing images to be expected from certain crystal defects of which four general classes may be distinguished.

(1) A locally varying strain field (dislocation, misfitting precipitate, etc.).

(2) A planar defect like a stacking fault at the junction of two undistorted regions of the foil.

(3) Voids or gas bubbles in the foil.

(4) Local changes in the extinction distance (section 3.2.3.1), for example coherent precipitates.

All of these situations are within the scope of the ideas expressed in sections 3.2.1, 3.2.2. Contrast calculations for strain field defects of type 1 generally require the numerical integration of the Darwin–Howie–Whelan equations in some form often using the Bloch wave concept because the time for computation is much reduced. However, the differential equations based on modified Bloch waves are particularly useful for slowly varying strain fields (Wilkens *et al.*, 1967; Chik *et al.*, 1967). Defects of the type (2) and (4) are not accompanied by lattice strains under ideal conditions and the best approach involves the solution of the Darwin–Howie–Whelan equations for the appropriate boundary conditions at the internal surface, that is the defect. This type of calculation is most easily performed using the scattering matrix approach (Howie and Whelan, 1961; Amelinckx, 1970).

Despite these different approaches equations (3.1) and (3.5) are useful because they contain a number of parameters that are important to the experimentalist.

(1) The reflecting plane vector $\boldsymbol{g}$.

(2) The deviation from the Bragg position s.

Both (1) and (2) are controlled by tilting the specimen.

(3) The extinction distance ξ_g (see section 3.2.3.1) which increases with increasing g and decreases with increasing $|s|$; ξ_g is often used in conjunction with s to describe the deviation from the Bragg position as $w = \xi_g s$.

(4) The anomalous absorption coefficient ANO $= \xi_g/\xi'_g$ which is a function of the operative reflection, the atomic number and structure of the material. The value of ANO for cubic materials has been calculated by Humphreys and Hirsch (1968). In general fringe images such as stacking faults are sensitive to the value of ANO and may even be used to determine it (Clareborough, 1971). However, dislocation images are relatively insensitive to small variations of ANO and a value of 0.1 is normally used in computation of contrast.

It is by careful control of (1) and (2) with the full knowledge of (3) and (4) that crystal defects may be quantitatively analysed.

3.3.1 *Experimental Conditions for Quantitative Analysis*

The following conditions must be satisfied experimentally for quantitative analysis as described in sections 3.4–3.14, 3.21 except where specifically stated otherwise. Different experimental conditions are described for the remaining sections and the reader is referred to them for details.

(1) Images should always be produced under *two-beam dynamical conditions* so that the preceding theory may be quantitatively applied.

(2) In BF images deviation from the Bragg position, s should be small and positive (bright Kikuchi line just outside diffraction spot, see figure 2.37(c)). Under these conditions both better transmission and sharper clearer contrast are obtained than at $s = 0$ or $-$ve, see figure 3.2. Indeed for s – ve the background intensity is very low. Values of $w = \xi_g s \sim 0.2$–1.0 may be used as an approximate guide. (See section 2.10.2 for methods of measuring s.)

(3) In dark field the deviation from the Bragg position may be up to ± 1 but, if comparison is to be made with bright field images, specific values of w may be required depending on the case under consideration (see later sections).

(4) Thin areas < 2–$3\xi_g$ should be avoided because significant rearrangement of mobile crystal defects occurs (Hirsch *et al.*, 1967) particularly if the friction stress on dislocations is low (metals and alloys with f.c.c. or c.p.h. crystal structure).

(5) Regions of rapidly changing thickness should be avoided if the detailed image contrast is to be studied because of the marked changes in background intensity produced by thickness fringes (see section 3.2.3.1).

(6) The most suitable specimen thickness for observation at 100 kV under all reflections are those 5–$8\xi_g$ thick, where ξ_g is the extinction distance of a low-index reflection.

(7) Where maximum penetration is important, careful selection of the operative reflection is essential because penetration depends upon the operative reflection even in pure metals. For example in hexagonal metals $\{2\bar{2}00\}$-type reflections are more intense and give better penetration than $\{1\bar{1}00\}$-type reflections. Furthermore, systematically absent reflections which are present because of double diffraction, for example (0001) and $\{\bar{1}2\bar{1}2\}$ in hexagonal metals, also give poor penetration. Finally, in ordered materials superlattice reflections may also be weak leading to poor penetration and diffuse images because ξ_g is large and w is therefore usually large.

3.3.2 *Recognition of Dynamical and Kinematical Diffracting Conditions in the Electron Microscope*

Although the dynamical theory of electron diffraction describes most images from crystalline specimens in the electron microscope, kinematical

Table 3.1 Recognisable features of SADP and images for dynamical and kinematical diffracting conditions

SADP		BF image	
Dynamical	Kinematical	Dynamical	Kinematical
bright Kikuchi lines very close to strong diffracted spot such that $w = -1 \rightarrow +1.0$, see figure 2.37(c)	bright Kikuchi lines some distance from strong diffracted beam $w \gtrsim \pm 1.0$	s + ve well defined; thickness fringes following the contours of the edge of the specimen, section 3.2.3.1, figure 3.2(d)	few thickness fringes BF, except 1–2 very near edge of specimen, figure 3.2(g)
		a high-contrast image is obtained, figure 3.2(d)	a low-contrast image is obtained, figure 3.2(g)
		a slight overall graininess of the background is visible in many materials, figure 3.2(d)	the overall nature of the image is diffuse, figure 3.2(g)